Journal of Nuclear Materials 408 (2011) 45–53

Contents lists available at ScienceDirect

Journal of Nuclear Materials

journal homepage: www.elsevier.com/locate/jnucmat

Influence of ageing on the quasistatic fracture toughness of an SS 316(N) weld at ambient and elevated temperatures

G. Sasikala *, S.K. Ray [1]

Materials Technology Division, Indira Gandhi Center for Atomic Research, Kalpakkam 603 102, India

ARTICLE INFO

Article history:
Received 23 November 2009
Accepted 1 November 2010

ABSTRACT

The leak before break analysis of SS 316L(N) components of the prototype fast breeder reactor requires the elastic plastic fracture toughness parameter J for 0.2 mm crack extension, $J_{0.2}$, especially for the welds, at the operating temperatures. The J–R curves for the welds produced using the consumable developed by Indira Gandhi Centre for Atomic Research, were determined in the as-welded condition as well as after thermal ageing (923 K/4200 h) conditions at 298 K and 643 K, using unloading compliance method for 298 K and normalization method for 643 K. The aged material exhibited pop-in crack extensions of magnitudes that, according to ASTM E1820 standard, could be ignored for multi-specimen data analysis for determining $J_{0.2}$. Therefore, for this condition, J_{nom}–Δa curves were established using the multiple specimen method and also single specimen normalization method; for the latter, a modification earlier developed by the authors for accounting for small pop-in crack extensions was used. The value of $J_{0.2}$ from both methods showed excellent reproducibility. Ageing is seen to reduce the toughness of this material considerably at both the testing temperatures.

© 2010 Elsevier B.V. All rights reserved.

1. Introduction

For the high temperature structural components of the 500 MWe FBR under construction at Kalpakkam, a low carbon (0.03 wt.% max) nitrogen-bearing (0.06–0.08 wt.%) variant of the AISI type 316, designated as SS 316L(N), has been chosen in view of its combination of good high temperature mechanical properties, compatibility with coolant liquid sodium, good weldability, and resistance to intergranular stress corrosion cracking (IGSCC) in chloride and caustic environments. Consumables for welding the SS 316L(N) components of 500 MWe FBR were developed indigenously by Indira Gandhi Centre for Atomic Research. The weld deposit is specified to contain 3–7% δ ferrite to balance between resistance to hot cracking during welding, and embrittlement of the weld metal during elevated temperature (>823 K) prolonged service exposure because of transformation of δ ferrite to carbide and embrittling intermetallic phases such as σ, η, and χ etc. (for a review, see e.g. Ref. [1] and references cited therein).

The safe operation of the component depends on leak before break (LBB) justification., i.e., it has to be demonstrated that in case of any defect present in the component, detectable leak of the fluids will take place well before a catastrophic failure of the components such that safe shut down and/or repair can be undertaken without causing loss of life or extensive damage to the system. For the LBB justification of the welded components made of SS 316L(N), the elastic plastic fracture toughness (J) values for 0.2 mm crack extension, $J_{0.2}$, of the welds at the operating temperatures are required. Austenitic stainless steels are generally well known for their high toughness values [2]. For example, for a modified type 316L austenitic stainless steel base metal, J_{Ic} value as high as high 2 MJ m^{-2} at ~300 K, decreasing to ~1.2 MJ m^{-2} at 823 K has been reported [3]. However, in view of the embrittlement of the weld metal on extended thermal ageing, LBB justification of the components to the end of life would require the properties after accelerated ageing conditions to simulate the end of life condition of the weld. Therefore, a detailed study has been undertaken to characterize the quasistatic J–R curves for the indigenously developed SS 316(N) weld material at both ambient and service temperatures and also to assess its degradation after simulated service exposure. The material properties data provided in the RCC-MR design code [4] includes J values for different extents of crack growth for medium and advanced ageing conditions. This paper reports the results for the SS 316(N) weld material at 298 K and 643 K in the as-welded and advanced ageing (i.e., >4000 h at 923 K) conditions.

2. Experimental

2.1. Material and specimen preparation

Weld pads of approximate dimensions 500 × 400 × 12 mm, were prepared by shielded metal arc welding process. The

* Corresponding author. Tel.: +91 44 27480500x22178; fax: +91 44 27480118.
E-mail address: gsasi@igcar.gov.in (G. Sasikala).
[1] Currently retired.

0022-3115/$ - see front matter © 2010 Elsevier B.V. All rights reserved.
doi:10.1016/j.jnucmat.2010.11.001

schematic diagram of the weld pad indicating the position of the specimens is shown in Fig. 1. The weld pads were subjected to radiography to ensure absence of any unacceptable welding defects. The chemical composition of the weld metal is given in Table 1. In the as-welded condition, the weld metal had a duplex microstructure with ~5.5 FN δ ferrite (as measured by magne gauge) distributed uniformly in the austenite matrix in a vermicular morphology (Fig. 2a). It may be noted that at least in some locations, the δ ferrite phase forms an interconnected network. Specimen blanks were subjected to thermal ageing at 923 K for 4200 h. The microstructure of the aged weld metal is shown in Fig. 2b. It may be noticed that all the δ ferrite has transformed to $M_{23}C_6$ carbides and intermetallic phases. Magne gage measurements on the aged samples confirmed that the transformation of δ ferrite was complete.

Ten millimeters thick compact tension (CT) specimens for quasistatic fracture testing were fabricated from the aged blanks with the notch placed such that the crack plane is in the weld region (Fig. 3). The specimen design for 298 K testing is presented in Fig. 3a. For 298 K tests, a stiff COD gage with metallic arms was used, while that for the high temperature tests, had long quartz rod arms. Therefore, a small modification was required in the specimen design for high temperature, with integral knife edge only on one side and a flat surface on opposite side in order to avoid any torque on the quartz rod arms (Fig. 3b). Instead of conventional chevron notch, a straight wire EDM cut slot (diameter ~0.2 mm) was used as crack starter, because it was found that fatigue precracking was considerably easier and also faster with this type of crack starter notch. The specimens were pre-cracked in fatigue at ambient temperature following the prescription of ASTM E1820-01 [5], to achieve initial crack depth ratio of $a_0/W \sim 0.46$–0.5. Then the test specimens were side grooved to 20% net depth (1 mm deep groove on either surface along crack growth path with 45° flank angle and 0.25 mm root radius).

2.2. Fracture testing

The fracture tests were conducted at 298 K and at 643 K. For high temperature tests, the specimens were thermally equilibrated for about 30 min at the test temperature before commencing the test. The single specimen unloading compliance method was chosen for the 298 K test, while monotonic ramp test was adopted for high temperature. High resolution load (P), load line displacement (LLD) and actuator stroke data were captured using digital voltmeters with $6\frac{1}{2}$ digit resolution interfaced with a GPIB card and a PC, at time resolution of ~0.5 s. For all tests, a constant actuator displacement rate of 0.2 mm/min was used. However, for the intermittent unloading segments in the unloading compliance tests, a slower rate of 0.1 mm/min was chosen to ensure adequate number of data points for the compliance determination. This was necessitated by the limitation in data acquisition interval.

Since the unloading compliance method is not reliable at high temperatures and online crack length measurement system was not available during these tests, four specimens of the aged material were tested at 643 K, in order to establish the J_{nom}-R curves by the multiple specimen method. In addition, the data from the high temperature tests were analysed using the normalization data reduction technique as per ASTM E 1820, Appendix A15 [5]. For the as-welded material, however, only normalization method was chosen.

The fracture-tested samples were again fatigue cracked at ambient temperature before pulling them open to complete fracture. This post-test fatigue cracking was found to significantly enhance the definition of crack front and thus precision in measurement of the final crack length. The initial and final crack lengths were determined optically using the nine-point average method according to the ASTM standards. For this an optical microscope equipped with an X–Y stage with a digital display of 0.001 mm resolution was used.

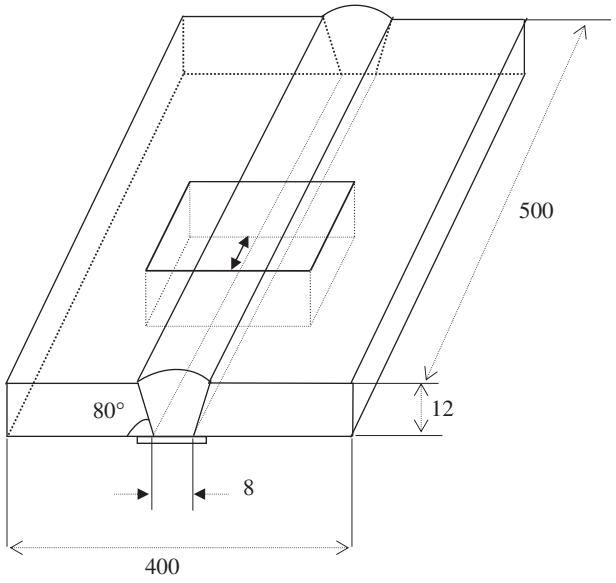

Fig. 1. Schematic of the weld pad with position of CT specimens indicated. Arrow indicates the orientation of the notch. All dimensions are in mm.

3. Results and discussion

3.1. Flow properties

The theoretical basis for J-integral parameter assumes rate-independent plasticity. At high temperature, however, for many materials this assumption need not be valid. Therefore, it was confirmed for the aged material at 643 K, by carrying out tensile tests at two strain rates differing by an order of magnitude, viz., 1.33×10^{-3} and $1.33 \times 10^{-4}\,s^{-1}$. Since, the results indicated that the material can be considered to be rate-insensitive at this temperature, tensile properties for other conditions were determined at a strain rate of $1.33 \times 10^{-4}\,s^{-1}$. These are presented in Table 2.

3.2. Fracture morphology

Scanning electron microscopic examination was carried out on the fracture surfaces of the tested samples. The scanning electron microscopic pictures of both as-welded and aged materials at 298 K and 643 K are presented in Figs. 4 and 5 respectively. It may be noted that in both material conditions and testing temperatures, fracture is predominantly by void nucleation and growth, as indicated by the general dimpled structure of the fracture surface. However, in the aged material, some pockets of brittle fracture with featureless, cleavage-like appearance suggesting pockets of brittle fracture were observed at both test temperatures (Figs. 4b and 5c). The as-welded material, as already mentioned in Section 2.1, has a duplex microstructure of δ ferrite + austenite. In Fig. 2a, the dark lines are δ ferrite and the white regions austenite. The orientation of δ ferrite in the weld is along the heat flow direction, which varies from bead to bead in a multipass weld, and results in a complex orientation distribution along the length of the weld pad. Fracture takes place along the δ ferrite regions where the second phase particles of brittle intermetallic phases that result from the transformation of δ ferrite, initiate voids/cracks mainly by

Table 1
Chemical composition of SS 316(N) weld (wt.%) and δ ferrite (FN) content of the deposited weld metal.

C	Si	Mn	Cr	Ni	Cu	Co	N	Mo	P	S	Nb	V	δ Ferrite
0.05	0.46	1.4	18.5	11.1	0.21	0.06	0.08	1.9	0.025	0.006	<0.07	0.075	5.5 FN

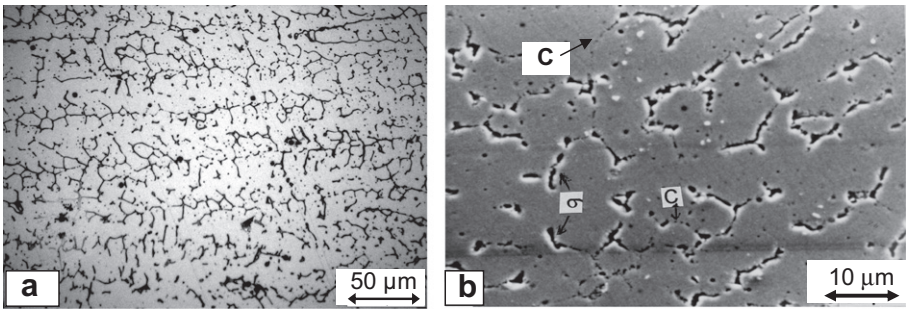

Fig. 2. Microstructure of the weld metal. (a) As-welded condition showing δ ferrite (dark) and austenite (white) regions. (b) After ageing for 4200 h at 923 K with carbides (C) and sigma phase (σ) indicated.

decohesion at the interface or by cracking of the particle itself, and coalesce without considerable local plasticity. Also, the locations where the secondary arms of dendrites originate provide a larger area on the fracture surface. Thus, there are isolated, flat featureless regions on the fracture surface. The appearance of the crack-like voids (shown by arrows) suggest that they form at sigma phase particles. The brittle (cracked) particles observed in these regions were analysed by EDAX and confirmed to be σ phase (Fig. 5d). Further, it may be noted that the dimples in the aged material (Figs. 4b and 5c) are generally smaller than those in the as-welded material (Figs. 4a and 5a), compared to that in the aged material despite the difference in magnification of these figures.

3.3. FEM study to determine the blunting line slope

ASTM E1820-01 [5] recommends the slope of the initial crack blunting line $J/\Delta a = M \cdot \sigma_f$ corresponding to elastic-ideal plastic behaviour of the specimen material, where σ_f is the flow stress of the material $((\sigma_y + \sigma_{UTS})/2)$. The minimum value of $M = 2$; however, it is recommended that for highly work hardening materials, a value as high as 4 may be used, provided it is justified by the data. To ascertain the value of M to be used, an elastic finite element simulation of crack blunting behaviour was carried out; tensile data for the aged SS 316(N) weld material generated at the test temperature was used in this. From FEM modeling for a non-growing crack with a tip radius of 1 μm, an M value of 2.098 was obtained, close to the ASTM specified minimum value of 2. Therefore, in the present work, a value of 2 has been consistently used for all the analyses.

3.4. Fracture test results at 298 K

The intermediate crack lengths during the tests were determined from the compliance of the specimen obtained from the unloading segments and the compliance crack length relations for this geometry (Eq. A 2.12) provided in ASTM E1820 [5]. The J values were computed following ASTM E1820 (Section A2.4.2.2) using Eqs. (1)–(3) as shown below:

$$J = J_{el} + J_{pl} \tag{1}$$

$$J_{(i)} = \frac{K^2_{(i)}(1-\nu^2)}{E} + J_{pl(i)} \tag{2}$$

$$J_{pl(i)} = \left\{ J_{pl(i-1)} + \left(\frac{\eta_{(i-1)}}{b_{(i-1)}} \right) \cdot \frac{A_{pl(i)} - A_{pl_{(i-1)}}}{B_N} \right\} \cdot \left[1 - \gamma_{(i-1)} \frac{a_{(i)} - a_{(i-1)}}{b_{(i-1)}} \right] \tag{3}$$

where J_{el}, J_{pl} – the elastic and plastic components of J, K – the stress intensity factor, ν – Poissons ratio, A_{pl} – instantaneous area under load–displacement curve, $\eta = 2.0 + 0.522\frac{b}{W}$ and $\gamma = 1.0 + 0.76\frac{b}{W}$. The subscripts i and $i-1$ indicate the current and previous measurements respectively. The J-Δa curves for the as-welded and aged specimens at 298 K are presented in Fig. 6a and b respectively. The $J_{0.2}$ values are 249 and 151 kJ m^{-2} respectively for the as-welded and advanced ageing conditions, indicating a reduction in the toughness of about 40% at 298 K due to ageing.

3.5. Fracture test results for 643 K

The P-LLD responses for the as-welded and aged materials were different at 643 K. While the P-LLD plot for the sample in as-welded condition was continuous, those for all the tests on the aged samples exhibited sudden load drops corresponding to pop-in crack extensions. Load drops sharply at a pop-in, and then increases rather rapidly through a sharp transient regime, beyond which its variation becomes more "regular". Pop-in crack extensions are observed in many materials [6–9], and have generally been ascribed to combinations of loading and crack tip conditions, plus local brittle zones. The fact that the "regular" P-LLD variation is rapidly re-established following a pop-in crack extension indicates that after pop-in crack extension, "regular" plastic zone is re-established at the crack-tip quite rapidly. Therefore, except very close to pop-in, the P-LLD data are not affected because of the sudden crack extension, and for all practical purposes, the data beyond the pop-in need not be "corrected" for the pop-in crack extension. For the as-welded material multiple specimen testing was not adopted; since no pop-in was observed, only the normalization method was chosen.

3.5.1. Multiple specimen data analysis for the aged material

Applying the ASTM E1820-01 criterion, pop-in crack extensions for the present data would be considered to be small, and therefore can be neglected in multiple specimen data analysis based upon

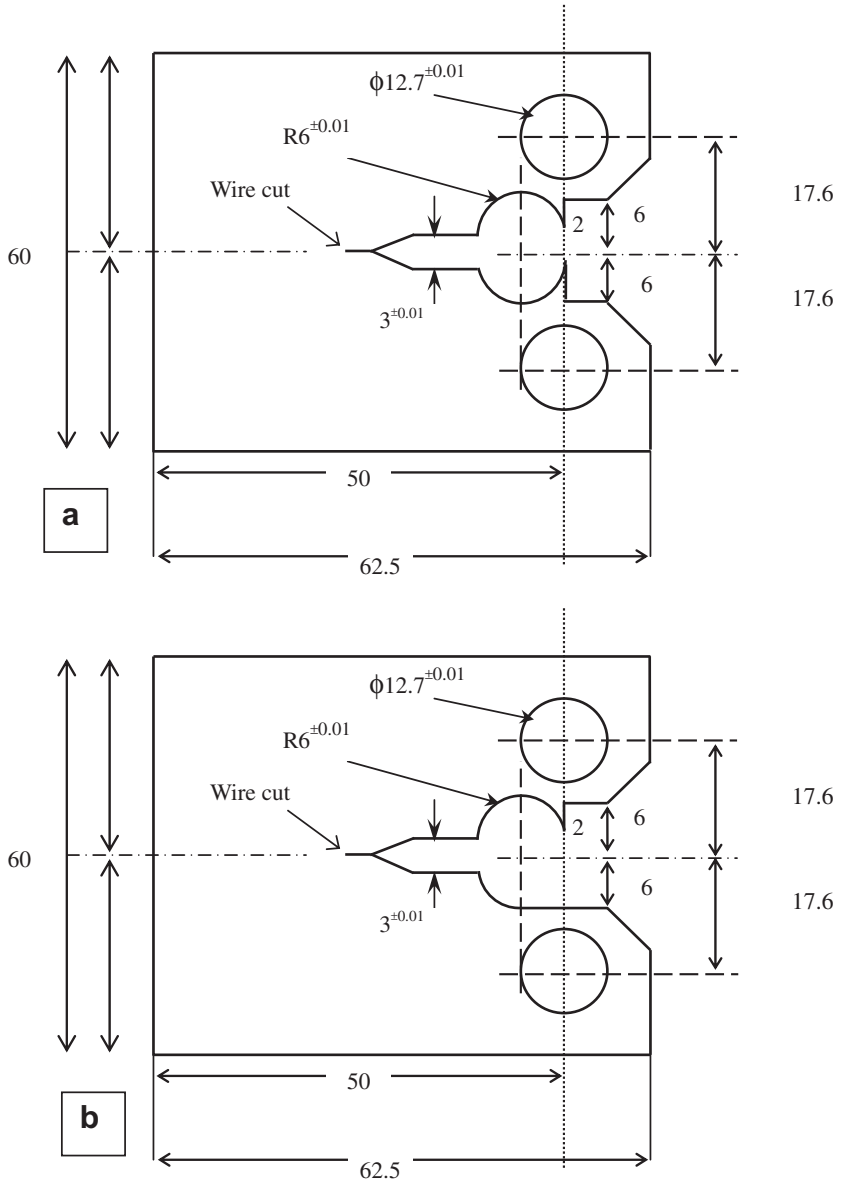

Fig. 3. Schematic diagram of the CT specimens used for the fracture tests at (a) 298 K and (b) 643 K.

$$J_{nom} = \frac{K^2(1-\nu^2)}{E} + \frac{\eta_{pl}A_{pl}}{B_N b_0} \tag{4}$$

which ignores variation of J due to crack growth. Here K is the stress intensity factor, ν the Poisson's ratio, E the elastic modulus, η_{pl} is the plastic η-factor, B_N the net thickness, b_0 the initial ligament length, and A_{pl} the area under the load (P) – plastic component of LLD v_p plot, with v_p computed ignoring crack growth. Appropriately, this method is used for determining $J_{0.2}$ where this variation can be ignored, but cannot be used for determining the J-resistance curve (J-Δa plot). It may be reiterated that this method requires continuity of the J-Δa plots across pop-in crack extensions, which must therefore be small. The J_{nom}–Δa curve obtained using multiple specimen method of data analysis is given in Fig. 7. The data were least square fitted to a power law of the form $J_{nom} = C \cdot \Delta a^n$; the values of the constants were $C = 307.6 \pm 6.04$ and $n = 0.4726 \pm 0.016$. Note that even though the number and disposition of the data generated do not conform to the requirements of the ASTM multiple specimen method, the constants C and n are well-determined. The value of $J_{0.2}$ obtained from this plot is 243 ± 8 kJ mm^{-2}.

Table 2
Tensile Properties of SS 316(N) weld in as-welded and aged conditions at a nominal strain rate 1.33×10^{-4} s^{-1}.

Temperature, K	Material	Yield stress, MPa	UTS, MPa	% Uniform elongation
298	As-welded	466	658	17.5
	Aged	421	692	9.0
643	As-welded	294	481	9.9
	Aged	225	546	16.9

3.5.2. The single specimen normalization method

The basis of the single specimen normalization method of Landes and coworkers [10–12] is the principle of separation of variables, expressed as:

$$P_N \equiv \frac{P}{G} = H\left(\frac{v_p}{W}\right) = \left(\frac{v_p}{W}\right) \cdot \frac{\left[L + M\left(\frac{v_p}{W}\right)\right]}{N + \left(\frac{v_p}{W}\right)};$$
$$G = WB\left[\frac{W-a-\Delta a}{W}\right]^{\eta_{pl}} \tag{5}$$

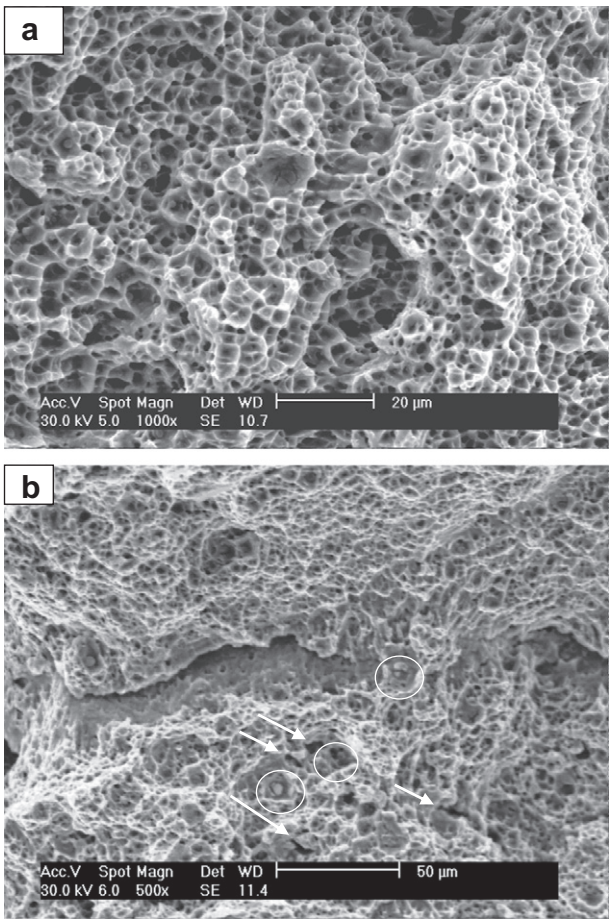

Fig. 4. (a) Scanning electron micrographs of the fracture surface of the specimens tested at 298 K, showing (a) general dimpled feature of the as-welded material (b) intermittent regimes of brittle fracture in the aged material. The cracked particles are shown in circles and the crack-like voids are indicated by white arrows.

In Eq. (5), L, M, N are fitting constants. For a few ferritic pressure vessel steels, data generated with specimens with blunt non-growing cracks with wide range for a/W values showed that the variable separation in Eq. (5) obtains except at very low values for v_p/W, and also justify this functional form. With L, M and N known *a priori*, for any pair of P-LLD data, the corresponding crack growth Δa can be determined, whence J can be determined as $J = J_{el} + J_{pl}$ from the values for its elastic and plastic components J_{el} and J_{pl}, using prescription of ASTM E1820-01 for analyzing data from single specimen unloading compliance method. ASTM E1820-01 Appendix A15 prescribes a method (using a slightly different form for the function H above, with four, rather than three fitting constants) of determining the fitting constants for the H function from the P-LLD data by considering initial effective crack growth due to plastic blunting of the crack-tip, and the final crack length corresponding to the starting point of unloading, determined optically from the fractured specimen. The main attraction of this method is that a single specimen is adequate and on-line crack length measurements are not necessary, which considerably reduce the test burden in terms of number of specimens or complexity of testing, and yet reliable J-resistance curves can be established. It was therefore decided to explore this method for estimating $J_{0.2}$, using the results from multiple specimen analyses as objective criteria to assess the single specimen estimation method.

There are however some additional considerations. The ASTM E1820-01 Appendix A15 prescription is based on a round robin test and analysis campaign with a bridge steel with considerably lower toughness ($J_{0.2} \approx 100$ kJ m^{-2}), tested in servohydraulic machines at high actuator speeds [13]. As such the viability of the functional form for H in the case of a highly work hardening high toughness austenitic steel may be open to question. Again, this prescription does not deal with the issue of pop-in crack extension, and indeed asserts that "The normalization method is not applicable for low toughness materials tested in large specimen sizes where large amount of crack extension can occur without measurable plastic load line displacement". The bridge steel used in the round robin test did not show pop-in crack extension, but did occasionally show de-lamination fracture and very non-uniform crack growth, which however did not seem to invalidate the analysis procedure.

In the tests at 643 K in the present study, the as-welded material did not show pop-in behaviour and the normalization method could be applied directly to the P-LLD data. The J–R curves obtained for the as-welded material at 643 K is presented in Fig. 8. It may be noted that the $J_{0.2}$ value at 643 K is higher compared to that obtained at 298 K presented in the previous section. However, the J–R curve at 298 K (Fig. 6a) is steeper compared to that at 643 K.

Ray and Sasikala [14] have adopted two alternative methods for J–R curve estimation from load (P)–displacement (v) data that shows pop-in behaviour. These basically assume two limiting types of "small" and "large" pop-in crack extensions, in the context of development of crack tip plastic zone during loading immediately following a pop-in crack extension event, and appropriately integrate with the normalization method. The present data were analyzed using the small pop-in assumption and the results are reported here. Consider a scenario where pop-in crack extension is vanishingly small. In this case pre- and post-pop-in crack tip plastic zones must match. In other words, for small pop-in crack growth, the J-resistance curve should be continuous, with possible local disturbances for pop-ins, and when this is enforced in data analysis, discontinuity in the $P_N - v_p/W$ plot is a measure of the extent by which pop-in crack extension differs from the "vanishingly small" assumption, and $P_N - v_p/W$ data, excluding the segment clearly identifiable with transient following pop-in crack extension, can be used for the normalization procedure. As noted earlier, the multi-specimen data analysis procedure (Section 3.5.1.) implies continuity of the J-Δa plots, which corresponds to this small pop-in crack growth assumption.

Fig. 9 shows typical plots of $P_N - v_p/W$ obtained using the ASTM E1820-01 Appendix 15 procedure, modified for use with a "small" pop-in assumption. It may be noted that there is a considerable specimen-to-specimen scatter in these plots. The corresponding J-Δa curves, Fig. 10, however, are seen to be bunched together. The J values for different extents of crack growth from each of these four single specimen J-Δa curves are given in Table 3. For fixed Δa levels, the data fall within a scatter band of ±5% except for the $J_{0.5}$ for sample number 4. Including the data for this sample, the scatter band increases to ±8 %. As indicated in Table 3, these are also similar to the corresponding J_{nom} values determined using the multiple specimen method up to 1.5 mm crack growth. These results confirm the viability of the method developed here for J estimation procedure for the case of data showing "small" pop-in crack extension behaviour.

3.6. Validity of $J_{0.2}$ values determined as J_{Ic}

The elastic plastic fracture toughness J_{Ic} is a thickness-independent material toughness property that corresponds to the highest crack tip constraint conditions characterized by the Hutchinson-Rice-Rosengren crack tip fields. The ASTM E1820-01 indicates two criteria:

1. The maximum J-integral measurement capacity of a specimen given by $J_{max} = \min(b_0\sigma_f/20,\ B\sigma_f/20)$, and

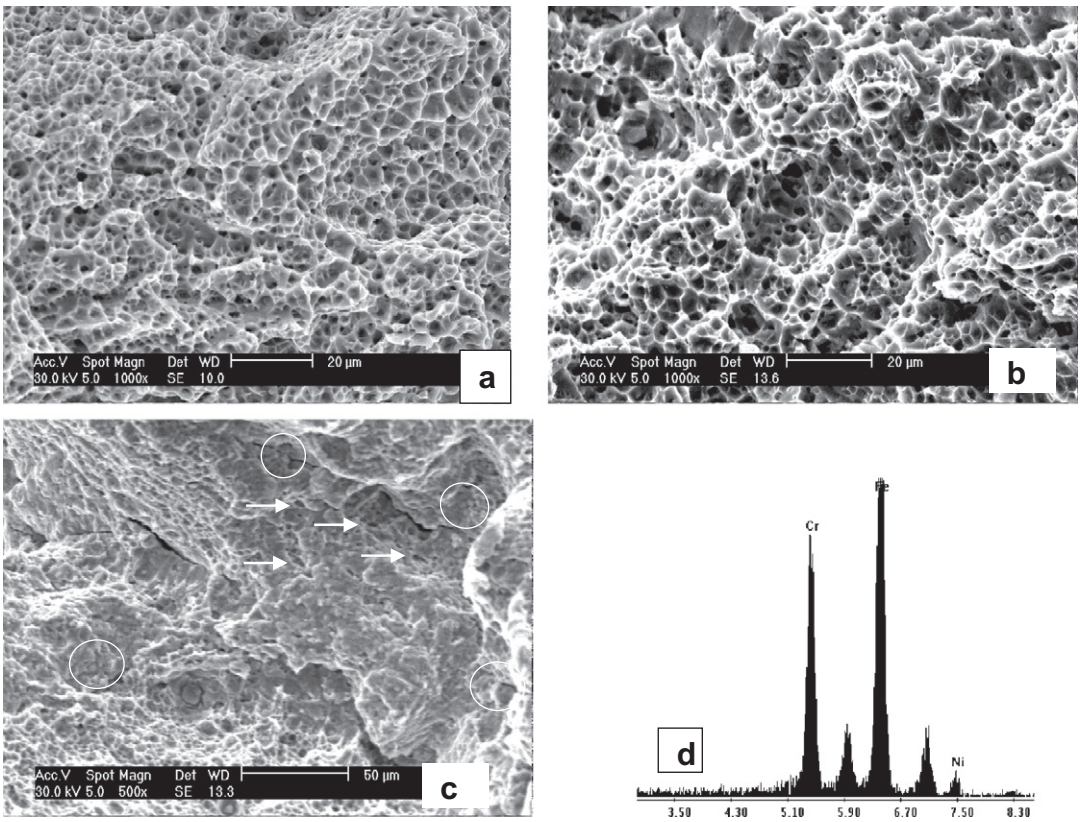

Fig. 5. (a–c) Scanning electron micrographs of the fracture surface of specimens tested at 643 K. (a) The typical (ductile dimpled) feature of the as-welded sample, (b) ductile dimpled structure, the typical general feature of the fracture surface of the aged material, (c) the intermittent local brittle zones in aged material and (d) the typical EDAX spectrum of particles shown encircled in (c) in the brittle region. The crack-like voids are indicated by white arrows.

2. Qualification of $J_{0.2}$ as elastic plastic fracture toughness J_{Ic}, which requires $J_{Ic} = J_{0.2} < \min(b_0\sigma_f/25,\ B\sigma_f/25)$.

The GKSS practice (EFAM GTP 94, see [15]) prescribes that fracture properties for initiation and growth are size-independent as long as $B \geqslant 20J/\sigma_f$ and the ligament is in dominant bending condition. For a 10 mm thick CT specimen, this turns out to be the same as the J_{max} criterion of ASTM, since $b_0 > 10$ mm. The values according to the three criteria are presented in Table 4. It may be noted that the $J_{0.2}$ determined here at 298 K for the as-welded material does not qualify as J_{Ic} by the ASTM criterion, though it is lower that the J capacity of the specimen and meets the GKSS criterion. However, the $J_{0.2}$ determined for the aged material at 298 K meets all the three validity criteria. On the other hand, for the testing temperature of 643 K, the $J_{0.2}$ determined here for both the as-welded and aged materials do not qualify as J_{Ic} by any of these criteria. These $J_{0.2}$ values, however, can be used in integrity assessment procedure like CEGB R6 [16] for component thickness of 10 mm, and should be conservative for lower thickness values. It may, however, be noted that the multiple specimen J–R curves up to 4 mm crack growth obtained for a high toughness SS 304 base material tested at 700 K, did not show any thickness dependence [2].

3.7. Comparison of the results with literature data

The J values obtained in this study for the aged material at both temperatures are much higher than those indicated in RCC-MR design documents [4]; in this document, for this class of welds in the advance aged condition, the J values for 0.2, 1.0 and 3.0 mm crack growth respectively are (i) 78, 182 and 325 kJ m^{-2} at 293 K (ii) 40, 105 and 239 kJ m^{-2} at 643 K. However, it may be noted that RCC-MR uses $J/(\sigma_f \cdot \Delta a) = 4$ for the crack tip blunting. Even if this value were to be used, from Figs. 6b and 7, $J_{0.2}$ values would have been significantly higher than the RCC-MR value. Another observation is that the $J_{0.2}$ values in the present study increased from 298 to 643 K, whereas, the data given in RCC-MR suggests otherwise. Sensitivity of these values for the method adopted for establishing the J–R curves needs to be examined. Comparison for the as-welded material is not presented here since the RCC-MR does not give the corresponding values.

The SS 316(N) weld investigated here is specially developed for welding nuclear grade SS 316 L(N) components for PFBR applications with stringent specifications. The minimum impact toughness is specified as Charpy U energy (C_U) 70 J cm^{-2} in the as-welded condition and 30 J cm^{-2} after an embrittling treatment of 100 h ageing at 1023 K. The values actually obtained were 76 and 40 J cm^{-2} respectively [17]. Also, the C_U values for this weld after ageing for various durations in the temperature range 923–1023 K have been correlated to the % transformation of δ ferrite [18]. 99% of the δ ferrite had transformed by 100 h ageing at 1023 K, and 95% by 500 h ageing at 923 K; the corresponding C_U values were 40 and 50 J cm^{-2} respectively. Chung [19] has correlated the room temperature Charpy V (C_V) values to J_{Ic} at 563 K for cast duplex stainless steels with more than 15% δ ferrite. Using Chung's results and ignoring the difference in constraint effects in U and V notch geometries in Charpy specimens, for room temperature C_U value of 40 J cm^{-2}, a J_{Ic} value of ~180 kJ m^{-2} is expected for the present material that generally agrees with $J_{0.2}$ from Fig. 6 with $J/(\sigma_f \cdot \Delta a) = 4$, but significantly higher than the RCC-MR value.

Generally, austenitic welds (308, 16-8-2, SS 316) prepared using shielded metal arc (SMA) procedure exhibited poorer toughness ($J_{Ic} \approx 100$ kJ m^{-2}) compared to those prepared by gas tungsten

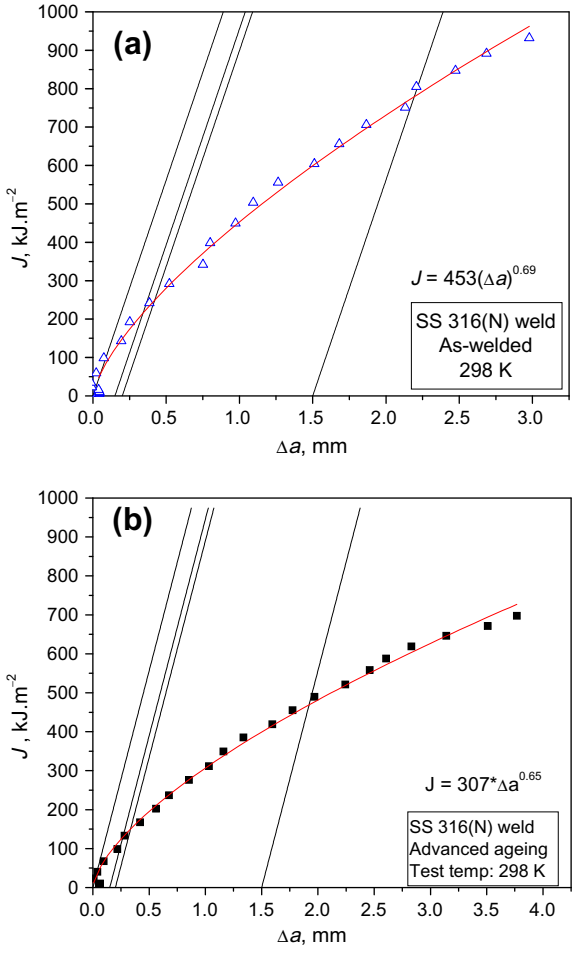

Fig. 6. *J–R* curves obtained from unloading compliance tests at 298 K for SS 316(N) weld material in (a) as-welded and (b) advanced ageing conditions.

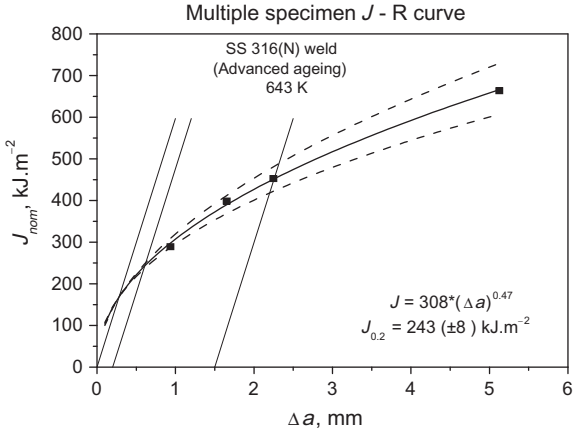

Fig. 7. The J_{nom}–Δa curve for the aged material from multiple specimen data analysis. The blunting lines are also shown. The solid line represents the fitted curve indicated in the graph and the dotted lines, the 95% confidence interval for the fit. The value for $J_{0.2}$ from this plot is 243 ± 8 kJ m^{-2}.

arc (GTA) or gas metal arc (GMA) welding procedures ($J_{Ic} \approx 300$ kJ m^{-2}) [2,20–24]. This was attributed to the better inclusion parameters (lower content, smaller size and larger spacing) of the GTA welds compared to those of SMA welds [2,23]. In this class of welds, fracture is dominated by ductile tearing [2,24], with microvoid nucleation at particles, followed by their growth and coalescence. In welds with high inclusion contents, these

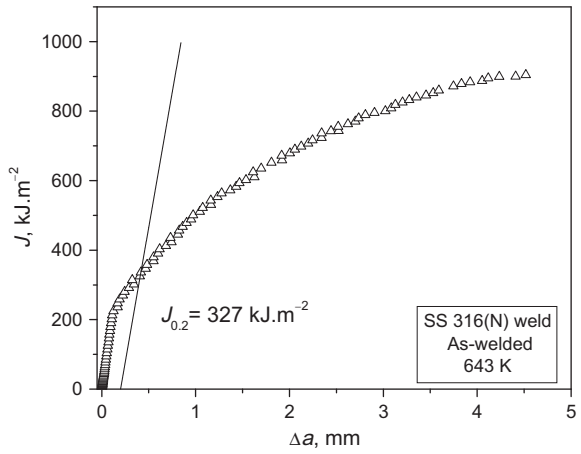

Fig. 8. Single specimen *J–R* curves for the as-welded material obtained using normalization method.

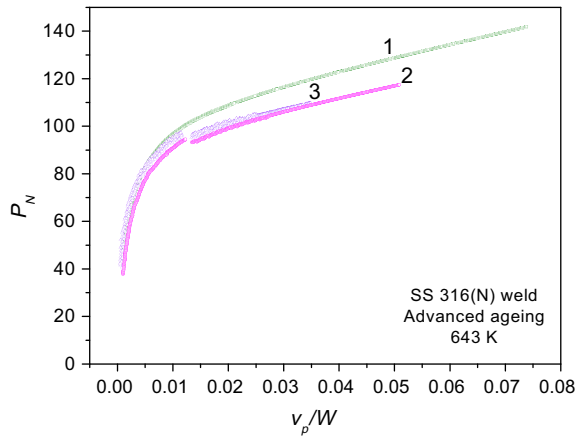

Fig. 9. Plots of P_N (normalized load) versus normalized v_p (plastic displacement)/W corrected for crack extension from normalization method modified with small pop-in assumption.

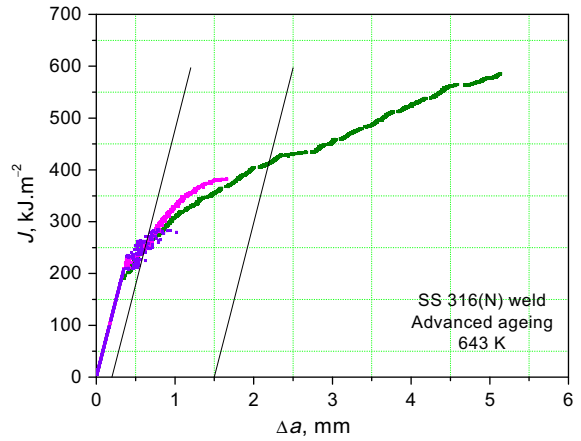

Fig. 10. Single specimen *J–R* curves obtained using normalization method with "small" pop-in assumption.

inclusions serve as easy void nucleating sites where as in welds with low inclusion contents, the δ ferrite (or its transformation products) and small inclusions allow nucleation only after considerable plastic deformation, thus leading to high toughness. When inclusions are favored sites for nucleation, microvoids

Table 3
Comparison of J values for various extents of crack growth for the SS 316(N) weld in the advanced ageing condition.

Temperature, K	Specimen no.	J values (kJ m^{-2}) for crack growth in mm				
		0.2	0.5	1.0	1.5	2.0
298	1*	151	249	365	466	555
643	1#	245	312	365	413	435
	2#	250	339	386	–	–
	3#	253	290	–	–	–
	4#	252	339	401	427	–
	Multiple specimen (J_{nom} values)	243	310.5	390	452	504

* Unloading compliance method.
\# Normalization method.

Table 4
Comparison of the $J_{0.2}$ values with the validity limits by ASTM criteria and GKSS practice.

Temperature, K	Material	ASTM		GKSS $B\sigma_{ff}/20$	$J_{0.2}$ kJ m^{-2}
		J_{max}	$J_{Ic,max}$		
298	As-welded	281	225	281	249
	Aged	278	222.6	278	151
643	As-welded	193.75	155	193.75	327
	Aged	192.75	154	192.75	250
					243*

* J_{nom} from multiple specimen analysis.

preferentially nucleate at these inclusions (rather than at the transformation products of δ ferrite) even after prior thermal ageing. In thermally aged low inclusion welds on the other hand, the transformation products, carbides and intermetallic phases, are expected to serve as preferential sites for void nucleation, leading to higher toughness. It may be noted that the silicon content in the GTA welds with low inclusion density and high toughness is comparable (less than 0.5% [22,23]) with that for the weld in the present study (0.46%). Mills [2] has reiterated the role of silicon on inclusion content. The general uniform and fine dimples observed on the fracture surface of the weld metal in the present case (Figs. 4 and 5) suggests that fine precipitates rather than inclusions serve as the sites for microvoid nucleation.

Therefore, the observed excellent toughness after advanced ageing of the present weld suggests the following scenario. To start with, the material has a low inclusion content and therefore the precipitates are the preferred sites for nucleation of microvoids. In the nitrogen-bearing weld, $M_{23}C_6$ type carbides are the first to form on ageing, and their coarsening is very sluggish due to the presence of nitrogen which forms complexes with chromium and reduce the chromium diffusivity [1,25]. The resultant microstructure contains fine carbonitride and Cr_2N precipitates. The intermetallic phases can form only after all the nitrogen and carbon have precipitated, and therefore presence of N delays precipitation and coarsening of these phases. The fine and uniformly distributed precipitates continue to act as the nucleation sites in the aged material, but since these require extensive plastic deformation, leading to the excellent high temperature fracture toughness observed in the present material. Further studies including detailed metallographic and fractographic investigations are required to confirm this conjecture.

4. Conclusions

1. J–R curves were established for SS 316(N) weld at 298 and 643 K in the as-welded condition as well as after extensive ageing equivalent to advanced ageing according to RCC-MR design code.
2. Ageing is found to lead to a significant reduction in toughness of this material; however, comparison of the J values for different extents of crack growth with those given in RCC-MR for this class of welds confirm that the weld in the present study have significantly high toughness.
3. The aged material tested at 643 K exhibited pop-in crack extensions; a modified normalization procedure was adopted for analysis of the data; the mean value for $J_{0.2}$ obtained from this method ($\sim$243 kJ m^{-2}) was found to be in close agreement with that from multiple specimen method ($\sim$250 kJ m^{-2}).
4. Further, both multiple specimen analysis and single specimen analysis yield similar values for J up to 1.5 mm crack extension, thus validating the modified normalization procedure adopted here for treating data with pop-in.
5. According to the ASTM criterion of validity, the $J_{0.2}$ values obtained here at the operating temperature 643 K, cannot be considered as a material property and should be used only for components of thickness less than or equal to 10 mm. The results at 298 K, however, generally meet the validity criteria.
6. The excellent fracture toughness of the weld even after advanced ageing is likely to be attributed to the high cleanliness combined with presence of nitrogen.

Acknowledgements

The authors wish to acknowledge Mrs. M. Radhika, Physical Metallurgy Division, IGCAR, Kalpakkam for scanning electron microscopy. The encouragement and support from Dr. Baldev Raj, Director, Indira Gandhi Centre for Atomic Research are gratefully acknowledged.

References

[1] G. Sasikala, Creep deformation and fracture behaviour of type 316L(N) stainless steel and its weld metal, Ph.D. Thesis, University of Madras, 2001.
[2] W.J. Mills, Int. Mater. Rev. 42 (2) (1997) 45.
[3] K.G. Samuel, O. Gossmann, H. Huthmann, Int. J. Pre. Ves. Piping 41 (1990) 59.
[4] Design and Construction Rules for Mechanical Components of FBR Nuclear Islands, RCC-MR, Section I-Subsection Z: Technical Appendix A16, 2002.
[5] ASTM Standard Test Method for Measurement of Fracture Toughness, ASTM E1820-01, American Society for Testing of Materials, Philadelphia, 2001.
[6] S.K. Ray, G. Sasikala, Fracture toughness evaluation of modified 9Cr–1Mo steel (P91) plate, Internal Report PFBR/33130/DN/1022.
[7] Xin Long, Guangjun Cai, Mater. Sci. Eng. A270 (1999) 260.
[8] A. Nishimura, R.L. Tobler, H. Tamura, S. Imagawa, J. Yamamoto, Fusion Eng. Des. 42 (1998) 425.
[9] G. Sasikala, S.K. Ray, Mater. Sci. Eng., A 479/1–2 (2008) 105–111.
[10] R. Herrera, J.D. Landes, Fracture Mechanics: Twenty first Symposium, ASTM STP 1074, in: J.P. Gudas, J.A. Joyce, E.M. Hackett (Eds.), American Society for Testing & Materials, Conshohocken, Philadelphia, 1990, p. 24.
[11] J.D. Landes, Z. Zhou, K. Lee, R. Herrera, J. Test. Eval. 19 (4) (1991) 305.
[12] Z. Zhou, K. Lee, R. Herrera, J.D. Landes, elastic plastic fracture test methods: The user's experience, in: J.A. Joyce, (Ed.), American Society for Testing & Materials, Philadelphia, ASTM STP 1114, vol. 2, 1991, p. 42.
[13] J.A. Joyce, J. Test. Eval. 29 (4) (2001) 329.
[14] S.K. Ray, G. Sasikala, A tentative procedure for treatment of data with pop-in crack extension for J estimation, 2002, Unpublished results.
[15] K.H. Schwalbe, U. Zerbst, Y.J. Kim, W. Brocks, A. Cornec, J. Heerens, H. Amstutz, Report EFAM ETM 97, The ETM method for assessing the significance of crack-like defects in engineering structures, comprising the versions EPM 97/1 and EPM 97/2, GKSS Forschungzentrum Geesthacht GmbH, Geesthacht, 1998.
[16] I. Milne, R.A. Ainsworth, A.R. Dowling, A.T. Stewart, Assessment of Integrity of Structures Containing Defects, CEGB R/H/R6, Revision 3, February 1988, Central Electricity Generating Board, London.
[17] A.K. Bhaduri, G. Srinivasan, V. Ramasubbu, K. Shanmugam, A. Balasubramanian, P. Ramadasan, Development of indigenous modified E316-15 electrodes for shielded metal arc welding, PFBR/30000/EX/1046, May 2002.
[18] V. Shankar, G. Srinivasan, Weldability of an indigenously developed modified E316-15 weld metal – Hot cracking and toughness degradation on ageing, PFBR/30000/EX/1047, August 2003.
[19] H.M. Chung, Int. J. Pres. Ves. Piping 50 (1990) 179.
[20] D.J. Alexander, J.M. Vitek, S.A. David, in: International Trends in Welding Science and Technology, ASM international, Materials Park, Ohio, 1993.
[21] W.J. Mills, Trans ASME J Pressure Vessel Technology 109 (1987) 440–448.

[22] W.J. Mills, Fracture Toughness of Stainless Steel Welds, in Fracture Mechanics: Nineteenth Symposium, T.A. Cruise, (Ed.) ASTM STP 969, American Society for Testing & Materials, Philadelphia, 1988, pp. 330–355.
[23] I.J. O'Donnel, H. Huthmann, A.A. Tavassoli, Int. J. Pres. Ves. Piping 65 (1996) 209.
[24] W.J. Mills, in: Fracture Mechanics: Perspectives and Directions, Twentieth Symposium, ASTM STP 1020, American Society for Testing & Materials, Philadelphia, 1989.
[25] G. Sasikala, M.D. Mathew, K. Bhanu Sankara Rao, S.L. Mannan, Metall. Mater. Trans. A 31A (2000) 1175.